Theoretical Derivation of the Stochastic Behavior of a WCDMA Signal Measured With a Spectrum Analyzer

Christof Olivier and Luc Martens, *Member, IEEE*

***Abstract*—Frequency-selective measurements with a spectrum analyzer are the most obvious means to accurately measure the power of a communication signal. In this paper, models for the spectrum analyzer and for the wideband code division multiaccess (WCDMA) signal are described. Based on these models, the analytic expressions for the probability density function (PDF) of the displayed signal have been derived for the different detection modes [sample, root mean square (rms) and positive-peak detection] of the spectrum analyzer. Based on these theoretical considerations, the dependence of the mean and standard deviation of the measured signal on the observation time of the detector has been examined, which showed a good agreement with the simulated results.**

***Index Terms*—Code division multiaccess (CDMA), land mobile radio, modeling, spectral analysis, stochastic processes, uncertainty.**

I. Introduction

FREQUENCY-SELECTIVE measurements with a spectrum analyzer are the most common means to characterize the different communication signals present on a shared medium. Indeed, since the different types of signal and the different operators have each been assigned a distinct part of the frequency spectrum, spectrum analysis is the most obvious method to accurately measure the power of a communication signal. The application that is envisaged in this paper is the assessment of the exposure to electromagnetic fields around antennas, although the developed results can easily be applied to other domains. In the case of exposure assessment, the exposure levels of a broad range of signals have to be determined and compared to the exposure guidelines [1]–[3]. Several measurement procedures have been proposed to check the compliance with the exposure guidelines [4], [5] and are now being standardized [6]–[10]. The typical measurement setup in most of these procedures consists of an electric antenna that transduces the electromagnetic fields to a signal that is measured with a spectrum analyzer.

On the other hand, since each communication signal has its own characteristics, the actual settings of a spectrum analyzer may have a large impact on the accuracy and even on the correctness if the measured results are not interpreted properly. It is thus of prime importance to understand how a certain communication signal is measured by a spectrum analyzer and how the different settings of the spectrum analyzer influence the behavior of the measured signal.

In a previous paper [11], the authors have discussed the measurement issues that arise when mobile communication signals of the second generation (i.e., global system for mobile communications) are measured with a spectrum analyzer. Now that different operators have introduced the third-generation technology to provide an answer to the increasing number of subscribers and to the growing demand for bandwidth, the authors have extended the research to the measurement of the universal mobile telecommunications system (UMTS) signal. Analogous to [11], the focus will be on the fundamental achievable accuracy on the measurement of a UMTS signal, without taking into account other relevant factors for the accuracy, like thermal noise of the measurement equipment or the use of power control. In this paper, analytical expressions for the probability distributions of the wideband code division multiaccess (WCDMA)-based UMTS signal, measured with a spectrum analyzer, will be developed. This approach allows to comprehend the measured signal and to analyze what the influence is of the different settings of the spectrum analyzer on the measurement result and its accuracy. It also identifies the underlying reasons for a certain behavior of the measured signal.

It should be noted, however, that for the application to CDMA signals, frequency-selective measurements do not provide as much information as vector signal analyzers or real-time spectrum analyzers, where the measured electromagnetic signal can be resolved in the code domain. The method described in this paper can be applied when this equipment is not available to measure the total power present in a WCDMA signal. On the other hand, the general applicability of spectrum analysis to every modulated signal and the lower cost of spectrum analyzers remain important advantages when using frequency-selective measurements for exposure assessment. This is also emphasized by the introduction of new measurement equipment, where portable spectrum analyzers are combined with isotropic-field probes to enable a quick analysis of the exposure situation, together with a characterization of the different sources.

In the first paragraph, the models that have been developed for simulations and for the derivation of the analytical models,

Manuscript received October 27, 2004; revised October 13, 2005. The work of C. Olivier was supported by a Grant of the Fund for Scientific Research Flanders (F.W.O. -Vlaanderen).

C. Olivier is with tComLabs, Ghent B-9000, Belgium (e-mail: Christof.Olivier@intec.UGent.be).

L. Martens is with the Department of Information Technology, Ghent University, Ghent B-9000, Belgium.

Digital Object Identifier 10.1109/TIM.2006.870330

both for the spectrum analyzer as for the WCDMA signal, will be discussed. In the next paragraph, the analytical expressions for the stochastic description of the measured signal will be derived for the different operation modes of the spectrum analyzer. Finally, the dependence of the mean and standard variation on the measuring period will be determined and compared for the different detector modes.

II. Simulation Model

Since it would not be feasible to execute simulations with signals in the radio-frequency domain due to the high sampling rate that would be necessary, the models for the spectrum analyzer and for the UMTS signal are translated into the lowpass representation, which enables the use of moderate sample times to perform the simulations, and provides a convenient way to describe the signal displayed on the spectrum analyzer.

A. Spectrum-Analyzer Model

The model that has been used for the spectrum analyzer is the same as the model developed in [11]: The signal entering the spectrum analyzer is first mixed with the local oscillator, which provides the sweeping frequency. Next, it is sent through an intermediate filter or a resolution filter with a half-power bandwidth RBW, subsequently is passed to an envelope detector, and finally is fed into the detector, which–depending on the detector mode of the spectrum analyzer–returns a sample value of the signal, the maximum or minimum that has occurred since the previous sample time, or the rms value of the signal over the previous interval. The lowpass representation of the signal after the envelope detector $|s(t)|$ is mathematically given by

$$|s(t)| = \left| \frac{1}{\sqrt{2\pi}\sigma_{\mathrm{t}}} \int_{-\infty}^{+\infty} r(t+v) e^{-j2\pi \frac{v_{\mathrm{sw}}}{2}(t+v)^2} e^{-\frac{v^2}{2\sigma_{\mathrm{t}}^2}} dv \right| \quad (1)$$

where $r(t)$ is the lowpass representation of the signal entering the spectrum analyzer; v_{sw} is the sweep rate of the spectrum analyzer and has been defined as the ratio of the frequency span Δf_{sp} to the sweep time T_{sw}; and σ_{t} is the width of the resolution filter in the time domain. σ_{t} is related to the width σ_{f}, its dual in the frequency domain, and to the resolution bandwidth (RBW) by

$$\sigma_{\mathrm{t}} = \frac{1}{2\pi\sigma_{\mathrm{f}}} = \frac{\sqrt{\ln 2}}{\pi \mathrm{RBW}}. \quad (2)$$

To ensure that the resolution filter can reach the steady state, the sweep rate has to be limited to

$$v_{\mathrm{sw}} < \frac{\mathrm{RBW}^2}{c} \quad (3)$$

where c is a constant, depending on the type of the spectrum analyzer. For an analog resolution filter, c is typically 2.5 [12]. Depending on the detector mode, the value displayed on the screen of the spectrum analyzer at the end of the kth measurement interval (or frequency bin) of length T_s is given by

$$s_{\mathrm{m}}(kT_s) = \begin{cases} |s(kT_s)|, & \text{sample mode} \quad (4a) \\ \max_{t\in](k-1)T_s, kT_s]} |s(t)|, & \text{positive-peak mode} \quad (4b) \\ \min_{t\in](k-1)T_s, kT_s]} |s(t)|, & \text{negative-peak mode} \quad (4c) \\ \sqrt{\frac{1}{T_s}\int_{(k-1)T_s}^{kT_s} |s(t)|^2 dt}, & \text{rms mode.} \quad (4d) \end{cases}$$

The noise floor of the spectrum analyzer can be taken into account by adding a white Gaussian noise to the input signal $r(t)$. If the noise power has a power density of σ_n^2, the probability density function (PDF) of the noise signal before the envelope detector $n_s(t)$ will be a complex Gaussian distribution with mean (0, 0) and standard deviations on the real and imaginary part of $\sqrt{\sigma_n^2 \sqrt{\pi}\sigma_{\mathrm{f}}/2}$.

B. Model for the UMTS Signal

In UMTS, WCDMA is used as a multiaccess technique. For a general description of the WCDMA signal that is being used in UMTS, we refer to [13]. The actual parameters can be found in the standards from the 3rd Generation Partnership Project [14]–[17]. Since it is the purpose of this paper to provide insight in the behavior of a WCDMA signal measured with a spectrum analyzer, not all the features of the UMTS signal will be implemented, and thus, the discussed model will incorporate some important assumptions.

1) The chip stream is considered to be completely random, although it originates from the spreading and scrambling operation on a certain data stream. However, since the chip sequences are pseudorandom, the approximation of the chip stream as a completely random stream is acceptable.
2) Although power control is a very important property of the UMTS system, it is not included in this model. However, the model will be extended with power control during the future research.

The lowpass representation of the WCDMA signal is shown in Fig. 1. For each channel j, a random chip stream at a rate of 3.84 Mcps is generated, the in-phase and quadrature chips are each multiplied with their respective channel gain (g_j) and summed together. The combined symbol is subsequently sent through a pulse-shaping filter (with frequency transfer function $H_{\mathrm{PS}}(f)$), whereupon the in-phase and quadrature-phase branches are combined into the complex low-pass signal. Subsequent chips are mutually independent, as are the chips from different channels. The values of the chips are assumed to be equally probable between $\{1, -1\}$. The pulse-shaping filter $H_{\mathrm{PS}}(f)$ is given by [18]

$$H_{\mathrm{PS}}(f) = \begin{cases} T_{\mathrm{c}}, & |f| < \frac{1-\alpha}{2T_{\mathrm{c}}} \quad (5a) \\ 0, & |f| \geq \frac{1+\alpha}{2T_{\mathrm{c}}} \quad (5b) \\ T_{\mathrm{c}} \cos\left(\frac{\pi}{2\alpha} T_{\mathrm{c}} \left(|f| - \frac{1-\alpha}{2T_{\mathrm{c}}}\right)\right), & \text{otherwise} \quad (5c) \end{cases}$$

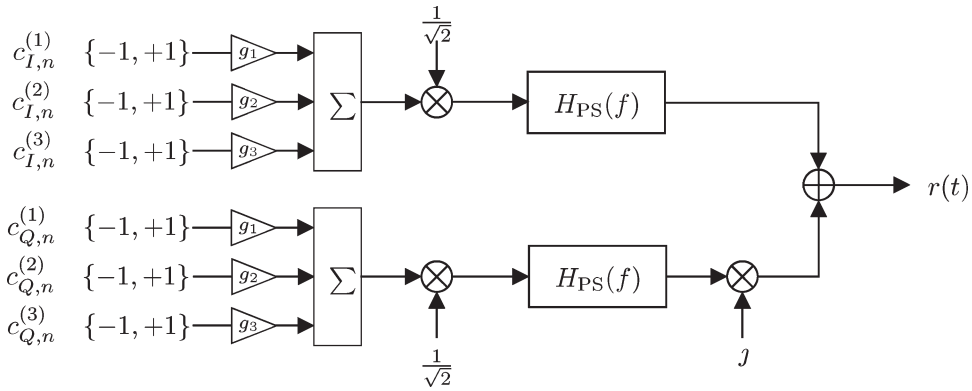

Fig. 1. Lowpass model for the WCDMA signal.

which is a root-raised cosine filter with a roll-off factor $\alpha = 0.22$, and the chip period $T_{\mathrm{c}} = 0.26\ \mu$s. Its time response will be denoted as $h_{\mathrm{PS}}(t)$.

A convenient representation of the lowpass WCDMA-signal is

$$r(t) = \sum_j \sum_n e^{j\phi_{c,n}^{(j)}} g_j h_{\mathrm{PS}}(t - nT_{\mathrm{c}}) \tag{6}$$

where $\phi_{c,n}^{(j)}$ denotes the phase of the nth chip pair $(c_{I,n}^{(j)}, c_{Q,n}^{(j)})$ of the jth channel, and g_j denotes the gain of the jth channel, as has been indicated in Fig. 1. Each chip pair is assumed to be equally probable and mutually independent from the other chip pairs, which yields to the probability distribution of the phases of the chips

$$\Pr\left[\phi_{c,n}^{(j)} = \frac{(2k+1)\pi}{4}\right] = \frac{1}{4}, \qquad k = 0,1,2,3 \tag{7}$$

C. Measured WCDMA Signal

If the WCDMA signal, given by (6), is measured by a spectrum analyzer, the signal after the envelope detector (1) can be written as

$$|s(t)| = \left| \sum_j g_j \sum_n e^{j\phi_{c,n}^{(j)}} p_n(t) \right| \tag{8}$$

where the stochastic part of the signal $|s(t)|$ is separated from the deterministic part, g_j is the gain of the jth channel, and $p_n(t)$ denotes the contribution of the nth chip to the signal. It has been defined as

$$\begin{aligned} p_n(t) &= p_n(nT_{\mathrm{c}} + t') \\ &= \frac{1}{\sqrt{2\pi}\sigma_{\mathrm{t}}} \int_{-\infty}^{+\infty} h_{\mathrm{PS}}(v + t') e^{-\frac{v^2}{2\sigma_{\mathrm{t}}^2}} e^{-j2\pi \frac{v_{\mathrm{sw}}}{2}(v+t'+nT_{\mathrm{c}})^2} dv. \end{aligned} \tag{9}$$

Since the argument $v + t' = \mathcal{O}(T_{\mathrm{c}})$ and because the sweep rate is bounded by (3), the phase term $1/2\, v_{\mathrm{sw}}(v+t')^2$ in the integral (9) can be neglected if $T_{\mathrm{c}} < \sigma_{\mathrm{t}}$. Then, the integral in expression (9) can be rewritten as the inverse Fourier transform of the pulse-shaping filter, multiplied with the resolution filter at the frequency under consideration $f_o = v_{\mathrm{sw}} n T_{\mathrm{c}}$, yielding for the pulse contribution function

$$\begin{aligned} p_n(nT_{\mathrm{c}} + t') \approx \frac{1}{\sqrt{2\pi}\sigma_{\mathrm{t}}} e^{-j2\pi \frac{v_{\mathrm{sw}}}{2}(nT_{\mathrm{c}})^2} \\ \mathcal{F}^{-1}\left[H_{\mathrm{PS}}(f + v_{\mathrm{sw}} n T_{\mathrm{c}}) H_{\mathrm{RB}}(f)\right](t') \end{aligned} \tag{10}$$

where $H_{\mathrm{RB}}(f)$ is the representation of the resolution filter in the frequency domain. If the used RBW is relatively small with respect to the width of the pulse-shaping filter, and the frequency under consideration is situated within the flat frequency part of $H_{\mathrm{PS}}(f)$ $(|f_o| < (1-\alpha)/2T_{\mathrm{c}})$, this pulse contribution function $p_n(t)$ can be approximated as

$$p_n(t) \approx \frac{T_{\mathrm{c}}}{\sqrt{2\pi}\sigma_{\mathrm{t}}} e^{-j2\pi \frac{v_{\mathrm{sw}}}{2}(nT_{\mathrm{c}})^2} e^{-\frac{(t-nT_{\mathrm{c}})^2}{2\sigma_{\mathrm{t}}^2}} \tag{11}$$

which is, thus, a time-shifted and phase-rotated version of the time-domain representation of the resolution filter.

III. Statistical Modeling

To derive the PDFs of the displayed measured signal (4), a brute-force technique is inappropriate: For the sample detector and low RBWs (e.g., 400 kHz), 15 different chips already contribute to the signal $|s(t)|$ leading to 4^{15} possible chip sequences that all have to be evaluated. In the case of multiple channels, the number of relevant chips grows linearly with the number of channels, and in the case of a positive-peak detector or rms detector, the chips occurring during the whole previous measurement interval should be known. The theoretical derivation of the statistical behavior is obviously a more appropriate method. In the following, we will develop the analytical expressions for the PDFs of the measured signal for the different detector modes.

A. Sampled Measured Signal

In the case of the sample detector, the measured signal $s_{\mathrm{m}}(kT_s) = |s(kT_s)|$ will not depend on the history of the signal before kT_s, so the statistical description of the sample measurement is equivalent to this of $|s(t)|$. Let the random variables $S_{\mathrm{r}}(t)$ and $S_{\mathrm{i}}(t)$ denote, respectively, the real and imaginary part

of $s(t)$. To calculate the probability distribution function of the signal $|s(t)|$, the joint PDF of the real and imaginary part should be known. This joint PDF can be found by making a detour along the joint characteristic function

$$\begin{aligned}\Psi_S(u,v) &= \mathrm{E}\left[\exp\left(ju\mathrm{Re}\left[S(t)\right]+jv\mathrm{Im}\left[S(t)\right]\right)\right] \\ &= \mathrm{E}\left[\exp\left(ju\mathrm{Re}\left[\sum_j g_j \sum_n e^{j\phi_{c,n}^{(j)}} p_n(t)\right]\right.\right. \\ &\qquad \left.\left. + jv\mathrm{Im}\left[\sum_j g_j \sum_n e^{j\phi_{c,n}^{(j)}} p_n(t)\right]\right)\right] \qquad (12) \\ &= \prod_j \prod_n \cos\left(ug_j \frac{p_{n,\mathrm{r}}(t)}{\sqrt{2}} - vg_j \frac{p_{n,\mathrm{i}}(t)}{\sqrt{2}}\right) \\ &\qquad \times \cos\left(ug_j \frac{p_{n,\mathrm{i}}(t)}{\sqrt{2}} + vg_j \frac{p_{n,\mathrm{r}}(t)}{\sqrt{2}}\right) \qquad (13)\end{aligned}$$

where $p_{n,\mathrm{r}}(t)$ and $p_{n,\mathrm{i}}(t)$ denote the real and imaginary part of $p_n(t)$, respectively. To obtain (13), the characteristic function of a sum of independent random variables has been written as the product of the characteristic functions of the individual random variables, which can easily be determined from the probabilities of the chips given by (7).

Using the exponential expansion for a cosine [19]

$$\cos(x) \approx \exp\left(-\frac{1}{2}x^2 - \frac{1}{12}x^4 - \frac{1}{45}x^6 - \cdots\right) \qquad (14)$$

which is valid for $x < \pi/2$, the characteristic function $\Psi_S(u,v)$ can be approximated by

$$\begin{aligned}\Psi_S^{(4)}(u,v) \approx \exp&\left(-\frac{1}{2}\sum_j g_j^2 \sum_n \frac{1}{2}\left(p_{n,\mathrm{r}}^2 + p_{n,\mathrm{i}}^2\right)\right) \\ &\times \exp\left(-\frac{1}{12}\sum_j g_j^4 \sum_n \left[\frac{1}{4}\left(p_{n,\mathrm{r}}^4 + p_{n,\mathrm{i}}^4\right)(u^4+v^4)\right.\right. \\ &\quad + p_{n,\mathrm{r}}p_{n,\mathrm{i}}\left(p_{n,\mathrm{i}}^2 - p_{n,\mathrm{r}}^2\right)uv(u^2-v^2) \\ &\quad \left.\left. + \frac{1}{4}p_{n,\mathrm{r}}^2 p_{n,\mathrm{i}}^2 u^2 v^2\right]\right) \qquad (15)\end{aligned}$$

where the dependence of $p_n(t)$ on time has been omitted for legibility; the superscript (4) indicates that the terms in u and v will only be retained up to the fourth order. It can be observed that if the terms of the fourth order are also disregarded, $\Psi_S(u,v)$ reduces to the joint characteristic function of two Gaussian variables. If there are multiple channels transmitted, the terms of the fourth order will be relatively less significant.

As it was mentioned above, the approximation is only valid if the argument of the cosine is smaller than $\pi/2$. This means that the characteristic function will only be accurate close to the origin $(u,v) = (0,0)$. As it is demonstrated in the Appendix, for large RBWs, the subsequent pulse contribution functions show a large decay in magnitude [see (70)–(73)], and not all the "moment energy" of the characteristic function is concentrated around the origin. The presence of "moment energy" away from the origin results in local oscillations in the PDF and in the cumulative distribution function (CDF), which is equivalent to a more discrete behavior of the signal. If the measured signal level is comparable to the noise floor of the signal level, this discrete behavior will be less pronounced.

The PDF of the sampled signal after the envelope detector can be found by changing from rectangular to polar coordinates, both in the probability $((x,y) \mapsto (r,\theta))$ as in the moment domain $((u,v) \mapsto (q,\phi))$. The joint PDF of the magnitude r and the phase θ can be found by applying the inverse two-dimensional (2-D) Fourier transform on the characteristic function

$$\begin{aligned}&f_{R\Theta}(r,\theta) \\ &= \frac{1}{2\pi}\int_0^\infty\int_0^{2\pi} \Psi_{R\Theta}(q,\phi)e^{-jq\cos(\phi)r\cos(\theta)}e^{-jq\sin(\phi)r\sin(\theta)}\,q\,d\phi\,dq\end{aligned} \qquad (16)$$

The marginal distribution of $|S(t)|$ can then be found by integrating over the phase

$$\begin{aligned}f_R(r) &= \frac{1}{2\pi}\int_0^{2\pi}\frac{1}{2\pi}\int_0^\infty rq\Psi_{R\Theta}(q,\phi)\int_0^{2\pi} e^{-jqr\cos(\phi-\theta)}d\theta\,dq\,d\phi \qquad (17) \\ &= \frac{r}{2\pi}\int_0^\infty qJ_0(rq)\int_0^{2\pi}\Psi_{R\Theta}(q,\phi)d\phi dq \qquad (18)\end{aligned}$$

where $J_0(\cdot)$ is the Bessel function of the first kind of zeroth order. Equation (18) can also be interpreted as $r/(2\pi)^2$ times the Hankel transform of the joint characteristic function in the polar domain, integrated over the angle. Transforming (15) to polar coordinates yields (19), shown at the bottom of the page.

$$\begin{aligned}\Psi_{R\Theta}^{(4)}(q,\phi) = \exp&\left(-\frac{q^2}{2}\sum_j g_j^2 \sum_n \frac{|p_n|^2}{2}\right) \\ &\times \exp\left(-\frac{q^4}{12}\sum_j g_j^4 \sum_n \left(\frac{3}{16}|p_n|^4 + \frac{1}{16}(p_{n,\mathrm{r}}^4 - 6p_{n,\mathrm{r}}^2 p_{n,\mathrm{i}}^2 + p_{n,\mathrm{r}}^4)\cos(4\phi) + \frac{1}{4}p_{n,\mathrm{r}}p_{n,\mathrm{i}}(p_{n,\mathrm{r}}^2 - p_{n,\mathrm{i}}^2)\sin(4\phi)\right)\right)\end{aligned} \qquad (19)$$

The integration of the characteristic function in the polar domain $\Psi_{R\Theta}(q,\phi)$ over the phase angle ϕ results in

$$b^{(4)}(q) = \int_0^{2\pi} \Psi_{R\Theta}^{(4)}(q,\phi)d\phi = 2\pi \exp\left(-\sum_j \sum_n \left(\frac{g_j^2|p_n|2}{4}q^2 + \frac{g_j^4|p_n|^4}{64}q^4\right)\right) I_0\left(\gamma^{(4)}(q)\right) \tag{20}$$

with $I_0(\cdot)$, the modified Bessel function of the first kind of zeroth order, and $\gamma^{(4)}(q)$

$$\gamma^{(4)}(q) = \frac{q^4}{48}\left(\sum_j g_j^4\right)\left[\left(\sum_n \left(p_{n,\mathrm{r}}^2 - p_{n,\mathrm{i}}^2\right)p_{n,\mathrm{r}}p_{n,\mathrm{i}}\right)^2 + \left(\frac{1}{4}\sum_n p_{n,\mathrm{r}}^4 + p_{n,\mathrm{i}}^4 - 6p_{n,\mathrm{r}}^2 p_{n,\mathrm{i}}^2\right)^2\right]^{\frac{1}{2}}. \tag{21}$$

The PDF of the sampled signal after the envelope detector $|s(t)|$ is thus given by $r/(2\pi)^2$ times the Hankel transform of $b^{(4)}(q)$.

If terms of order q^4 would have been neglected, the function $\gamma^{(2)}(q)$ would reduce to 0, and consequently, the function $b^{(2)}(q)$ would be approximated by a Gaussian form. Since the Hankel transform of a Gaussian function is given by the Rayleigh distribution, the second-order approximation of the marginal distribution $f_R(r)$ is

$$f_R^{(2)}(r) = \frac{2r}{\sum_j g_j^2 \sum_n |p_n(t)|^2}\exp\left(-\frac{r^2}{\sum_j g_j^2 \sum_n |p_n(t)|^2}\right). \tag{22}$$

This could be expected since, for moderate RBWs, a large number of chips contribute to the signal after the resolution filter. Hence, the real and imaginary parts of the signal could in a first approach be described as two mutual independent Gaussian distributions and, thus, the signal after the envelope detector, which is fed into the sample detector, is described by the Rayleigh distribution. Substituting (11) into the parameter of the Rayleigh distribution (22), applying the Poisson sum formula on $\sum_n \exp(-(t-nT_\mathrm{c})^2/(2\sigma_\mathrm{t}^2))$ and assuming that $\sigma_\mathrm{t} \gg T_\mathrm{c}$, the parameter of the Rayleigh distribution can be approximated as

$$\frac{1}{2}\sum_j g_j^2 \sum_n |p_n(t)|^2 \approx \frac{\sqrt{\pi}\sigma_\mathrm{f} T_\mathrm{c}}{2}\sum_j g_j^2 \tag{23}$$

which is, as it could be expected, proportional to the RBW of the signal and to the summed power of the different channels.

In Fig. 2, the PDF of the measured sample distribution of the WCDMA signal used in UMTS (5-MHz wide), measured with a 400-kHz wide resolution filter, is shown, calculated both with brute-force techniques and with the approximations (22) and (18). As it can be seen, the second-order distribution does not follow exactly the PDF predicted by the brute-force simulation. For larger levels r, the Rayleigh distribution overestimates the exact PDF, while the approximation of the fourth order remains valid.

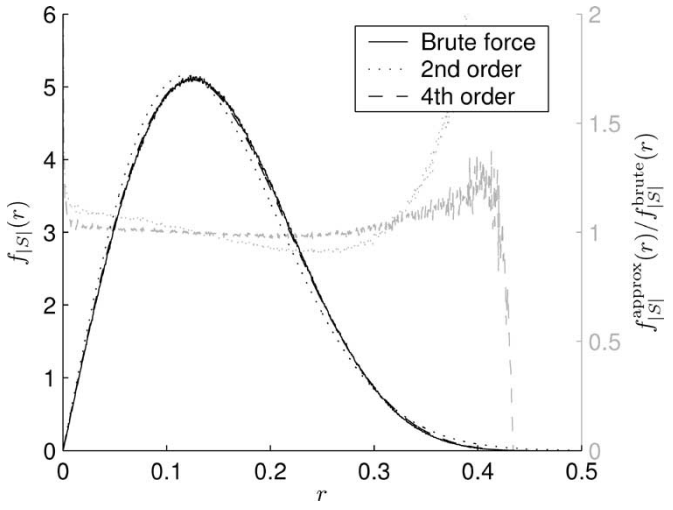

Fig. 2. PDF of the sampled measured sample for a WCDMA signal measured with a resolution filter of 400 kHz in the flat part of the pulse-shaping filter. The PDF obtained with brute-force simulations (solid line) is compared to the second-order (dotted line) and fourth-order approximations (dashed). The ratio between the approximations and the brute-force simulation is indicated in gray.

If the noise is taken into account, the characteristic function (19) should be multiplied with an additional factor $\exp(-q^2(\sigma_n^2\sqrt{\pi}\sigma_\mathrm{f}/4))$. The parameter of the Rayleigh distribution (23) will then be changed to

$$\frac{\sqrt{\pi}\sigma_\mathrm{f}}{2}\left(T_\mathrm{c}\sum_j g_j^2 + \sigma_n^2\right) \tag{24}$$

so that the contribution of the noise floor may be neglected if the spectral power density of the WCDMA signal is sufficiently stronger than the spectral power density of the noise.

B. RMS Measured Signal

To calculate the PDF of the signal measured with the rms detector, first, the statistical description of the mean-square (MS) signal $s_\mathrm{ms}(kT_s)$ will be derived. Using notation (8) for the signal before the detector, the MS signal becomes

$$s_\mathrm{ms}(kT_s) = \frac{1}{T_s}\sum_j \sum_{j'} g_j g_{j'} \sum_n \sum_{n'} e^{\jmath\phi_{c,n}^{(j)} - \jmath\phi_{c,n'}^{(j')}} \int_{(k-1)T_s}^{kT_s} p_n(t)p_{n'}^*(t)dt. \tag{25}$$

By using expression (9) for the pulse contribution functions $p_n(t)$, and changing the integration sequence, the integral in

the expression above can be rewritten as

$$\int_{(k-1)T_s}^{kT_s} p_n(t)p^*_{n'}(t)dt$$
$$= \frac{1}{2\pi\sigma_{\mathrm{t}}^2}\exp\left(-\jmath\pi v_{\mathrm{sw}}(n^2-n'^2)T_{\mathrm{c}}^2\right)\int_{-\infty}^{\infty}\Bigg[h_{\mathrm{PS}}(u')h_{\mathrm{PS}}(v')$$
$$\times e^{-\jmath\pi v_{\mathrm{sw}}(u'nT_{\mathrm{c}}-v'n'T_{\mathrm{c}})}\sqrt{\pi}\sigma_{\mathrm{t}}\exp\left(-\frac{(u'-v'+(n-n')T_{\mathrm{c}})^2}{2\sigma_{\mathrm{t}}^2}\right)$$
$$\times w_{\mathrm{erf}}\left(u'+v'+(n+n')T_{\mathrm{c}}-2(k-1)T_s\right)\Bigg]du'dv' \quad (26)$$

where $w_{\mathrm{erf}}(\cdot)$ is a window function determining which pulse functions $p_n(t)$ contribute to the MS signal. It has been defined as

$$w_{\mathrm{erf}}(u) = \frac{1}{2}\left(\mathrm{erf}\left(\frac{u}{2\sigma_{\mathrm{t}}}\right) - \mathrm{erf}\left(\frac{u-2T_s}{2\sigma_{\mathrm{t}}}\right)\right) \quad (27)$$

and can be approximated by a rectangular window over the interval $[0, 2T_s]$, provided that the inverse of the RBW is small compared to the measuring period T_s. This window function provides the condition on the chips that contribute to the MS signal of the kth measuring interval

$$(k-1)T_s < \frac{n+n'}{2}T_{\mathrm{c}} < kT_s. \quad (28)$$

Analogous to the approximation of the pulse contribution function (10), the integral of the pulse contribution functions can be estimated by

$$\int_{(k-1)T_s}^{kT_s} p_n(t)p^*_{n'}(t)dt$$
$$\approx \frac{1}{2\sqrt{\pi}\sigma_{\mathrm{t}}}e^{-\jmath 2\pi v_{\mathrm{sw}}(n^2-n'^2)T_{\mathrm{c}}^2}$$
$$\times \mathcal{F}^{-1}\Bigg[H_{PS}\left(f+\frac{v_{\mathrm{sw}}}{2}nT_{\mathrm{c}}\right)\exp\left(-\frac{f^2}{\sigma_{\mathrm{f}}^2}\right)$$
$$\times H_{PS}\left(f-\frac{v_{\mathrm{sw}}}{2}n'T_{\mathrm{c}}\right)\Bigg]\left((n-n')T_{\mathrm{c}}\right). \quad (29)$$

If the frequencies $\pm\{{}^{n}_{n'}\}T_{\mathrm{c}}(v_{\mathrm{sw}}/2)$ are located in the flat frequency part of the pulse-shaping filter, the pulse-shaping filter H_{PS} can be replaced by T_{c}. The measured MS value is then given by

$$s_{\mathrm{ms}}(kT_s) = \frac{T_{\mathrm{c}}^2}{T_s}\frac{1}{2\sqrt{\pi}\sigma_{\mathrm{t}}}\sum_j\sum_{j'}g_jg_{j'}\sum_n\sum_{n'}e^{\jmath\phi_{c,n}-\jmath\phi_{c,n'}}$$
$$\times e^{-\jmath\pi v_{\mathrm{sw}}(n^2-n'^2)T_{\mathrm{c}}^2}\exp\left(-\frac{(n-n')^2T_{\mathrm{c}}^2}{4\sigma_{\mathrm{t}}^2}\right). \quad (30)$$

By introducing a new set of indexes $(m = n+n', m' = n-n')$ (see also Fig. 3) and grouping the indexes of identical chips and channels, (30) can be rewritten as

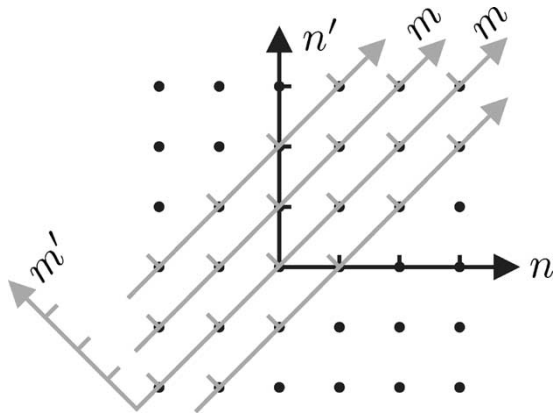

Fig. 3. Transition from the sum indexes (n, n') to the new indexes (m, m').

$$s_{\mathrm{ms}}(kT_s)$$
$$= \frac{T_{\mathrm{c}}^2}{T_s}\frac{1}{2\sqrt{\pi}\sigma_{\mathrm{t}}}\Bigg\{\sum_j g_j^2N_s + 2\sum_j g_j^2\sum_{m'>0}\exp\left(-\frac{m'^2T_{\mathrm{c}}^2}{4\sigma_{\mathrm{t}}^2}\right)$$
$$\times\sum_m\cos\left(\pi v_{\mathrm{sw}}mm'T_{\mathrm{c}}^2+\phi_{c,n}^{(j)}-\phi_{c,n'}^{(j)}\right)$$
$$+2\sum_j\sum_{j'\neq j}g_jg_{j'}\sum_{m'\geq 0}\exp\left(-\frac{m'^2T_{\mathrm{c}}^2}{4\sigma_{\mathrm{t}}^2}\right)$$
$$\times\sum_m\cos\left(\pi v_{\mathrm{sw}}mm'T_{\mathrm{c}}^2+\phi_{c,n}^{(j)}-\phi_{c,n'}^{(j')}\right)\Bigg\} \quad (31)$$

where m should satisfy the condition $2(k-1)T_s < mT_{\mathrm{c}} < 2kT_s$ and increases with 2 (as indicated in Fig. 3), whereas m' runs over all integers; N_s is the number of contributing chips and can be approximated by T_s/T_{c}. If the expected value of the MS value (30) is taken, the expected value reduces to the first term of (31), where the same channel is considered $(j = j')$ and $m' = 0$

$$\mathrm{E}\left[s_{\mathrm{ms}}(kT_s)\right] = \sum_j g_j^2\frac{T_{\mathrm{c}}^2}{T_s}\frac{N_s}{2\sqrt{\pi}\sigma_{\mathrm{t}}} \approx \sum_j g_j^2\frac{T_{\mathrm{c}}}{2\sqrt{\pi}\sigma_{\mathrm{t}}} \quad (32)$$

As it could be expected, the expected MS value is independent of the measuring period T_s and proportional to the RBW as to the sum of squared gains.

To obtain the PDF of the MS value, again the detour along the characteristic function is made. First, the characteristic function $\Psi_{\Sigma_m}(u)$ of the summation over m can be calculated. Since the phase differences between chips are mutually dependent, the characteristic function is the product of cosines

$$\Psi^{(4)}_{\Sigma_m}(u)$$
$$= \prod_m\cos\left(\frac{1}{2}\left(\cos\left(\pi v_{\mathrm{sw}}mm'T_{\mathrm{c}}^2\right)+\sin\left(\pi v_{\mathrm{sw}}mm'T_{\mathrm{c}}^2\right)\right)u\right)$$
$$\times\cos\left(\frac{1}{2}\left(\cos\left(\pi v_{\mathrm{sw}}mm'T_{\mathrm{c}}^2\right)-\sin\left(\pi v_{\mathrm{sw}}mm'T_{\mathrm{c}}^2\right)\right)u\right) \quad (33)$$

$$\approx \exp\left(-N_s\frac{u^2}{4}\right)\exp\left(-N_s\frac{u^4}{64}+\sum_m \frac{u^4}{192}\cos\left(\pi v_{\mathrm{sw}} m m' T_{\mathrm{c}}^2\right)\right) \tag{34}$$

where, again, (14) has been applied. Although, strictly speaking, it is not correct to consider the different sums over m as independent random variables, their mutual correlation will be very small for small index differences m' and a large number of contributing chips. Moreover, because of the term $\exp(-m'^2 T_{\mathrm{c}}^2/4\sigma_{\mathrm{t}}^2)$, the contribution of more distant chip pairs will be lower, especially for larger RBWs. This means that the assumption that the different summations over m are mutually independent is acceptable. In accordance to these considerations, the characteristic function of the summation over m' can be written as a product

$$\Psi_{\Sigma_{m'}}(u) \approx \prod_{m'} \Psi_{\Sigma_m}(A_{m'}u) \tag{35}$$

where $A_{m'}$ is $\exp(-m'^2 T_{\mathrm{c}}^2/4\sigma_{\mathrm{t}}^2)$. Analogously, the characteristic function of the MS signal can be derived by multiplying all characteristic functions $\Psi_{\Sigma_{m'}}(u)$ for the different channels. Again, the same objections are valid regarding to the independence of the variables. The fourth-order approximation of the characteristic function of the MS signal can thus be written as

$$\begin{aligned}
\Psi_{\mathrm{ms}}^{(4)}(u) = {} & \exp\left(\jmath\alpha\sum_j g_j^2 N_s u\right) \\
& \times \exp\left(-\alpha^2\left[\sum_j g_j^4 \sum_{m'>0} A_{m'}^2 \right.\right. \\
& \qquad \left.\left. + \sum_j\sum_{j'\neq j} g_j^2 g_{j'}^2 \sum_{m'\geq 0} A_{m'}^2\right] N_s u^2\right) \\
& \times \exp\left(-\alpha^4\left[\sum_j g_j^8 \sum_{m'>0} A_{m'}^4 \right.\right. \\
& \qquad \left.\left. + \sum_j\sum_{j'\neq j} g_j^4 g_{j'}^4 \sum_{m'\geq 0} A_{m'}^4\right] N_s \frac{u^4}{4}\right) \\
& \times \exp\left(\alpha^4\left[\sum_j g_j^8 \sum_{m'>0} A_{m'}^4 \sum_m \cos\left(\pi v_{\mathrm{sw}} m m' T_{\mathrm{c}}^2\right) \right.\right. \\
& \qquad + \sum_j\sum_{j'\neq j} g_j^4 g_{j'}^4 \sum_{m'\geq 0} A_{m'}^4 \\
& \qquad \left.\left. \times \sum_m \cos\left(\pi v_{\mathrm{sw}} m m' T_{\mathrm{c}}^2\right)\right] N_s \frac{u^4}{12}\right)
\end{aligned} \tag{36}$$

where α is $T_{\mathrm{c}}^2/(2\sqrt{\pi}\sigma_{\mathrm{t}} T_s)$. If, as a first approximation, only the terms of second order are retained, the probability distribution of the measured MS signal can be approximated by a Gaussian random variable with mean

$$\mu_{\mathrm{ms}} = \sqrt{\pi}\sigma_{\mathrm{f}} T_{\mathrm{c}} \sum_j g_j^2 \tag{37}$$

and standard variation

$$\sigma_{\mathrm{ms}}^2 \approx 2\alpha^2\left[\sum_j g_j^4 \sum_{m'>0} A_{m'}^2 + \sum_j\sum_{j'\neq j} g_j^2 g_{j'}^2 \sum_{m'\geq 0} A_{m'}^2\right] N_s \tag{38}$$

$$\approx \frac{\sqrt{2\pi}\sigma_{\mathrm{f}} T_{\mathrm{c}}^2}{2T_s}\left(\sum_j g_j^2\right)^2 = \frac{\mu_{\mathrm{ms}}^2}{\sqrt{2\pi} T_s \sigma_{\mathrm{f}}}. \tag{39}$$

To obtain the last expression, the sums of $A_{m'}$ are calculated with the Poisson sum formula and it is assumed that $\sigma_{\mathrm{f}} \ll 1/T_{\mathrm{c}}$. The expected MS value is proportional to the RBW and the summed power of the channels and is independent of the measurement period. The standard deviation on the MS value decreases with $\sqrt{T_s}$ and is proportional to the summed power of the channels. If the standard deviation on the MS value is considered relative to the mean value, it appears from (39) that the standard deviation is inversely proportional to the square root of the product of the measurement period and the RBW.

If again the contribution of the noise is taken into consideration, the MS value measured by the spectrum analyzer will be given by

$$s_{\mathrm{ms,noise}}(kT_s) = s_{\mathrm{ms}}(kT_s) + \frac{1}{T_s}\int_{(k-1)T_s}^{kT_s} |n_s(t)|^2\, dt \tag{40}$$

since the contribution from the signal and the contribution of the white noise can be considered as uncorrelated. Accordingly, the mean and the standard deviation on the MS signal are given by

$$\mu_{\mathrm{ms,noise}} = \mu_{\mathrm{ms}} + \mu_{\mathrm{noise}} = \sqrt{\pi}\sigma_{\mathrm{f}}\left(T_{\mathrm{c}}\sum_j g_j^2 + \sigma_n^2\right) \tag{41}$$

and

$$\sigma_{\mathrm{ms,noise}}^2 \approx \sigma_{\mathrm{ms}}^2 + \sigma_{\mathrm{noise}}^2 = \frac{\mu_{\mathrm{ms}}^2 + \mu_{\mathrm{noise}}^2}{\sqrt{2\pi}\sigma_{\mathrm{f}} T_s} \tag{42}$$

where for the standard deviation on the noise, it has been assumed that the measurement interval of the bin T_s is much longer than the answer of the resolution filter σ_{t}. Hence, if noise is present, it will be impossible to distinguish the contribution of the white noise to the measured signal from the WCDMA signal.

Once the PDF of the MS measurement is known, the PDF of the rms value is easily derived

$$f_{\mathrm{rms}}(r) = \frac{dF_{\mathrm{ms}}(r^2)}{dr} = 2r f_{\mathrm{ms}}(r^2) \tag{43}$$

$$f_{\mathrm{rms}}^{(2)}(r) = \sqrt{\frac{2}{\pi}}\frac{r}{\sigma_{\mathrm{ms}}}\exp\left(-\frac{(r^2-\mu_{\mathrm{ms}})^2}{2\sigma_{\mathrm{ms}}^2}\right) \tag{44}$$

with $F_{\mathrm{ms}}(r^2)$ as the CDF of the MS signal distribution.

C. Positive-Peak Signal

To calculate the PDF of the positive-peak signal, an analogous method to the one described in [20] will be followed. As it was demonstrated by Rice [21], the expected number of maxima $\bar{N}_{\max_{]t_0,t_1]}}(m)$ that a stochastic process $R(t)$ attains within the interval $]t_0, t_1]$ and that are above a certain level m is given by

$$\bar{N}_{\max_{]t_0,t_1]}}(m) = \int_{t_0}^{t_1} \int_{m}^{+\infty} p_{\max}(t, r)\, dr\, dt \tag{45}$$

where $p_{\max}(t_0, r_0)dt\, dr$ is the probability that a stochastic process $R(t)$ reached a local maximum in the region $]t_0, t_0 + dt] \times]r_0, r_0 + dr]$. $p_{\max}(t_0, r_0)$ can be calculated as

$$p_{\max}(t_0, r_0) = -\int_{-\infty}^{0} \ddot{r} f_{R\dot{R}\ddot{R}}(r_0, 0, \ddot{r}) d\ddot{r} \tag{46}$$

where $f_{R\dot{R}\ddot{R}}(r, \dot{r}, \ddot{r})$ is the joint PDF of the stochastic process $R(t)$, and $\dot{R}(t)$ is its first-order, and $\ddot{R}(t)$ its second-order derivative to time. As a consequence, the probability that an arbitrary peak ρ of the signal $R(t)$ in the interval $]t_0, t_1]$ lies above the level m is given by

$$\Pr[\rho > m] = \frac{\bar{N}_{\max_{]t_0,t_1]}}(m)}{\bar{N}_{\max_{]t_0,t_1]}}(0)} \tag{47}$$

which is the ratio of the expected number of maxima during the time interval $]t_0, t_1]$, that are larger than m, to the expected total number of maxima within the same interval. Since the positive-peak detector operates on the signal after the envelope detector, the positive-peak signal is restrained on the lower side by 0, and thus, $\bar{N}_{\max_{]t_0,t_1]}}(0)$ denotes the expected total number of maxima.

To derive the PDF of the positive-peak signal, the peak process (or the interarrival times between two successive maxima) should be known, which is difficult to analyze. However, if the assumption is made that successive maxima are mutually independent, analogous to [20], the problem can be easily solved. Let $M_{]t_0,t_1]}$ be the maximum measured signal over the interval $]t_0, t_1]$, then $M_{]t_0,t_1]}$ is equal to the maximum of all the peaks ρ_{i} that have occurred during the interval

$$M_{]t_0,t_1]} = \max_{1 \le i \le \bar{N}_{\max_{]t_0,t_1]}}(0)} \rho_{\mathrm{i}}. \tag{48}$$

If the period is sufficiently long, due to the law of large numbers, the number of maxima in the period will be equal, with probability 1, to its expected value $\bar{N}_{\max_{]t_0,t_1]}}(0)$. Since it has been assumed that the peaks are mutually independent, the cumulative distribution of $M_{]t_0,t_1]}$ is given by

$$F_{M_{]t_0,t_1]}}(m) = \Pr\left[\rho_{\mathrm{i}} \le m \quad \forall i : 1 \le i \le \bar{N}_{\max_{]t_0,t_1]}}(0)\right] \tag{49}$$

$$= \Pr\left[\rho \le m\right]^{\bar{N}_{\max_{]t_0,t_1]}}(0)} \tag{50}$$

$$= \left(1 - \frac{\bar{N}_{\max_{]t_0,t_1]}}(m)}{\bar{N}_{\max_{]t_0,t_1]}}(0)}\right)^{\bar{N}_{\max_{]t_0,t_1]}}(0)}. \tag{51}$$

The joint PDF of the signal, leaving the envelope detector and its first- and second-order derivatives to time, can be found in an analogous way to the calculation of the PDF of the sampled signal. The joint characteristic function in the Cartesian coordinates of the real and imaginary signals s_{r} and s_{i}, and their first and second derivatives $\dot{s}_{\mathrm{r}}$, $\ddot{s}_{\mathrm{r}}$, $\dot{s}_{\mathrm{i}}$, $\ddot{s}_{\mathrm{i}}$, respectively, is given by

$$\Psi_{S\dot{S}\ddot{S}}(u, \dot{u}, \ddot{u}, v, \dot{v}, \ddot{v}) = \prod_j \prod_n \cos\left(g_j \alpha_n(t)\right) \cos\left(g_j \beta_n(t)\right) \tag{52}$$

with

$$\alpha_n(t) = \frac{1}{\sqrt{2}} \left(u p_{n,\mathrm{r}}(t) + \dot{u}\dot{p}_{n,\mathrm{r}}(t) + \ddot{u}\ddot{p}_{n,\mathrm{r}}(t) + v p_{n,\mathrm{i}}(t) + \dot{v}\dot{p}_{n,\mathrm{i}}(t) + \ddot{v}\ddot{p}_{n,\mathrm{i}}(t)\right) \tag{53}$$

$$\beta_n(t) = \frac{1}{\sqrt{2}} \left(u p_{n,\mathrm{i}}(t) + \dot{u}\dot{p}_{n,\mathrm{i}}(t) + \ddot{u}\ddot{p}_{n,\mathrm{i}}(t) - v p_{n,\mathrm{r}}(t) - \dot{v}\dot{p}_{n,\mathrm{r}}(t) - \ddot{v}\ddot{p}_{n,\mathrm{r}}(t)\right) \tag{54}$$

where, again, the dotted functions denote the first-order time derivatives, and the double-dotted functions denote the second-order time derivatives. Once more, the second-order approximation of this product series is an exponential function, yielding

$$\Psi^{(2)}_{S\dot{S}\ddot{S}}(u, \dot{u}, \ddot{u}, v, \dot{v}, \ddot{v}) \approx \exp\left(-\frac{1}{2}\sum_j g_j^2 \sum_n \left(\alpha_n^2(t) + \beta_n^2(t)\right)\right) \tag{55}$$

$$\approx \exp\left(-\frac{1}{2}\mathbf{U}^{\mathrm{T}}\mathbf{\Gamma}\mathbf{U}\right) \tag{56}$$

where the second-order approximation was rewritten as the characteristic function of a six-dimensional multivariate Gaussian distribution with covariance matrix $\mathbf{\Gamma}$. $\mathbf{U}$ is given by $[u\ \dot{u}\ \ddot{u}\ v\ \dot{v}\ \ddot{v}]$. The corresponding PDF then becomes

$$f^{(2)}_{S\dot{S}\ddot{S}}(s_{\mathrm{r}}, \dot{s}_{\mathrm{r}}, \ddot{s}_{\mathrm{r}}, s_{\mathrm{i}}, \dot{s}_{\mathrm{i}}, \ddot{s}_{\mathrm{i}}) = \frac{1}{(2\pi)^3 |\mathbf{\Gamma}|} \exp\left(-\frac{1}{2}\mathbf{S}^{\mathrm{T}}\mathbf{\Gamma}^{-1}\mathbf{S}\right) \tag{57}$$

with $\mathbf{S} = [s_{\mathrm{r}}\ \dot{s}_{\mathrm{r}}\ \ddot{s}_{\mathrm{r}}\ s_{\mathrm{i}}\ \dot{s}_{\mathrm{i}}\ \ddot{s}_{\mathrm{i}}]$.

If the frequency under consideration $f_o = v_{\mathrm{sw}} n T_{\mathrm{c}}$ falls within the flat-frequency part of the pulse-shaping filter, the pulse contribution functions, and analogously their

time-derivatives, can be approximated by (11). The covariance matrix can then be written as

$$\mathbf{\Gamma} \approx \begin{bmatrix} \mathbf{\Gamma}_{\mathrm{r}} & \mathbf{0} \\ \mathbf{0} & \mathbf{\Gamma}_{\mathrm{i}} \end{bmatrix}. \tag{58}$$

The submatrices $\mathbf{\Gamma}_{\mathrm{r}}$ and $\mathbf{\Gamma}_{\mathrm{i}}$ are equal. They can be elaborated by using the Poisson sum formulas, and only retaining the terms independent of time (which can be done if $\sigma_{\mathrm{f}} \ll 1/T_{\mathrm{c}}$), yielding

$$\mathbf{\Gamma}_{\mathrm{r}} = \mathbf{\Gamma}_{\mathrm{i}} = \frac{T_{\mathrm{c}}}{2\sqrt{\pi}\sigma_{\mathrm{t}}} \sum_j g_j^2 \begin{bmatrix} \frac{1}{2} & 0 & -\frac{1}{4\sigma_{\mathrm{t}}^2} \\ 0 & \frac{1}{4\sigma_{\mathrm{t}}^2} & 0 \\ -\frac{1}{4\sigma_{\mathrm{t}}^2} & 0 & \frac{3}{8\sigma_{\mathrm{t}}^4} \end{bmatrix}. \tag{59}$$

It should be noted that if σ_{t} is chosen as the new time basis, and the signal levels are normalized to the root of the expected MS value $\sqrt{T_{\mathrm{c}} \sum_j g_j^2/(2\sqrt{\pi}\sigma_{\mathrm{t}})}$ [see (37)], a dimensionless distribution is obtained, independent of the chip rate or the RBW. From now on, these scaled variables will be indicated with a hat. The joint PDF of the signal after the envelope detector can be found by a transformation to polar coordinates. To calculate the function $\hat{p}_{\max}(\hat{t}, \hat{r})$, the marginal distribution $f_{\hat{R}\dot{\hat{R}}\ddot{\hat{R}}}(\hat{r}, 0, \ddot{\hat{r}})$ has to be known as

$$\begin{aligned} & f^{(2)}_{\hat{R}\dot{\hat{R}}\ddot{\hat{R}}}(\hat{r}, 0, \ddot{\hat{r}}) \\ &\quad = \int_{-\infty}^{\infty}\int_{-\infty}^{\infty}\int_{0}^{2\pi} \hat{r}^3 f_{\hat{S}\dot{\hat{S}}\ddot{\hat{S}}}(\hat{s}_{\mathrm{r}}, \dot{\hat{s}}_{\mathrm{r}}, \ddot{\hat{s}}_{\mathrm{r}}, \hat{s}_{\mathrm{i}}, \dot{\hat{s}}_{\mathrm{i}}, \ddot{\hat{s}}_{\mathrm{i}})\, d\hat{\phi}\, d\dot{\hat{\phi}}\, d\ddot{\hat{\phi}}\Big|_{\dot{\hat{r}}=0} \quad (60) \\ &\quad \approx \frac{4}{\pi^{\frac{3}{2}}} \exp\left(-\left(\frac{3}{2}\hat{r}^2 + 2\hat{r}\ddot{\hat{r}} + \ddot{\hat{r}}^2\right)\right) \hat{r}^{\frac{3}{2}} \sqrt{\ddot{\hat{r}}} K_{\frac{1}{4}}\left(\ddot{\hat{r}}^2\right) \quad (61) \end{aligned}$$

where $K_{1/4}(\cdot)$ is the modified Bessel function of the second kind of order 1/4. This normalized marginal distribution is independent of the RBW and the chip rate. Since the marginal distribution does not depend on time, the expected number of maxima with a level above the normalized value $\hat{m}$ can be written as

$$\begin{aligned} & \bar{N}_{\max_{]\hat{t}_0, \hat{t}_1]}}(\hat{m}) \\ &\quad \approx -(\hat{t}_1 - \hat{t}_0) \int_{\hat{m}}^{+\infty} \hat{r}^{\frac{3}{2}} \exp\left(-\frac{3}{2}\hat{r}^2\right) \\ &\qquad \times \int_{-\infty}^{0} \ddot{\hat{r}} \frac{4}{\pi^{\frac{3}{2}}} \exp\left(-(2\hat{r}\ddot{\hat{r}} + \ddot{\hat{r}}^2)\right) \sqrt{\ddot{\hat{r}}} K_{\frac{1}{4}}\left(\ddot{\hat{r}}^2\right) d\ddot{\hat{r}}\, d\hat{r} \quad (62) \\ &\quad \approx (\hat{t}_1 - \hat{t}_0) \bar{\nu}(\hat{m}) \quad (63) \end{aligned}$$

with $\bar{\nu}(\hat{m})$ denoting the expected rate of maxima above a normalized level $\hat{m}$ in a fixed time interval σ_{t}. The cumulative distribution of the maximum can then be written as

$$F^{(2)}_{\hat{M}_{]\hat{t}_0, \hat{t}_1]}}(\hat{m}) = \left(1 - \frac{\bar{\nu}(\hat{m})}{\bar{\nu}(0)}\right)^{\bar{\nu}(0)(\hat{t}_1 - \hat{t}_0)} \tag{64}$$

where only the exponent depends on time.

For long observation periods, the levels of the observed maxima will be located at the tails of the probability distribution $f_{\hat{R}}(\hat{r})$. This means that an accurate description of the tail distribution is essential to calculate the PDF of the positive-peak signal. This is achieved by also enclosing the fourth-order terms in the joint characteristic function for the real and imaginary parts of the signal (but not for their time derivatives). The inclusion of fourth-order terms involves the multiplication of the second-order approximation (56) with the function $G(\hat{u}, \hat{v})$, which is given by

$$\begin{aligned} G(\hat{u}, \hat{v}) = \exp\Bigg(& \frac{1}{12} \sum_j g_j^4 \sum_n \frac{1}{4} \left(\hat{u}\hat{p}_{n,\mathrm{r}}(\hat{t}) + \hat{v}\hat{p}_{n,\mathrm{i}}(\hat{t})\right)^4 \\ & + \left(\hat{u}\hat{p}_{n,\mathrm{i}}(\hat{t}) + \hat{v}\hat{p}_{n,\mathrm{r}}(\hat{t})\right)^4 \Bigg). \end{aligned} \tag{65}$$

The multiplication of the characteristic function with $G(\hat{u}, \hat{v})$ implies in the probability domain the convolution of the joint PDF with the inverse Fourier transform of $G(\hat{u}, \hat{v})$. After transforming to the polar-coordinate system, the fourth-order approximation of $\hat{p}_{\max}(\hat{r})$ is given by

$$\hat{p}^{(4)}_{\max}(\hat{r}) = \hat{r} \int_0^{\infty} \hat{s} J_0(\hat{r}\hat{s}) \tilde{g}(\hat{s}) \int_0^{\infty} \hat{p}^{(2)}_{\max}(\hat{q}) J_0(\hat{s}\hat{q})\, d\hat{s}\, d\hat{q} \tag{66}$$

with $\tilde{b}(\hat{s})$

$$\tilde{b}(\hat{s}) = \exp\left(-\frac{1}{16} \sum_n \frac{1}{4} |\hat{p}_n|^4 \hat{s}^4\right) I_0\left(\gamma^{(4)}(\hat{s})\right) \tag{67}$$

and $\gamma^{(4)}(\hat{s})$ is analogous to (21), but where the pulse-shaping functions are scaled to $\sqrt{\mu_{\mathrm{ms}}}$, and dually, the magnitude $\hat{s}$ is multiplied with $\sqrt{\mu_{\mathrm{ms}}}$.

In Fig. 4, the function $\bar{\nu}(\hat{m})$ is given for both the second- and fourth-order approximations (compared to simulations of the signal using the model described in Fig. 1). If longer observation periods T_s are considered, the behavior of (64) will be determined by the values of $\bar{\nu}(\hat{m})$ for large $\hat{m}$, and thus the second-order approximation of the behavior will no longer be valid. On the other hand, if multiple channels are transmitted, the second-order approximation will be relatively better compared to the single-channel case. Once the average mean rate of maxima $\bar{\nu}(\hat{m})$ is known, the CDF can easily be derived from (64).

Considering the internal noise of the spectrum analyzer, the second-order approximation of the cumulative distribution for the positive-peak detector will still be given by (64), where the levels, however, have to be normalized to $\sqrt{\mu_{\mathrm{ms,noise}}} = \sqrt{\sqrt{\pi}\sigma_{\mathrm{f}}(T_{\mathrm{c}} \sum_j g_j^2 + \sigma_n^2)}$, while the procedure to obtain the fourth-order approximation remains the same. This implies that the correction term for the fourth-order approximation will be relatively less important, and thus, the second-order approximation will be more accurate.

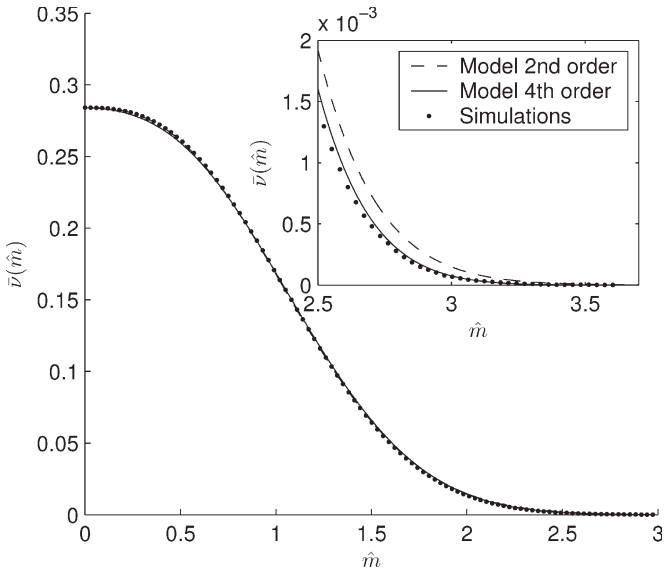

Fig. 4. Normalized expected rate of maxima $\bar{\nu}(\hat{m})$. Comparison between the mean number of maxima above the normalized level $\hat{m}$ obtained by simulations (•) and the mean number of maxima predicted by the second-order (dashed line) and the fourth-order models (solid line). The tail behavior of $\bar{\nu}(\hat{m})$ is shown in more detail in the inset. Simulations were executed during the interval 50–100 ms. The chosen sweep time was 500 ms, the frequency span was 6 MHz, and the RBW was 100 kHz.

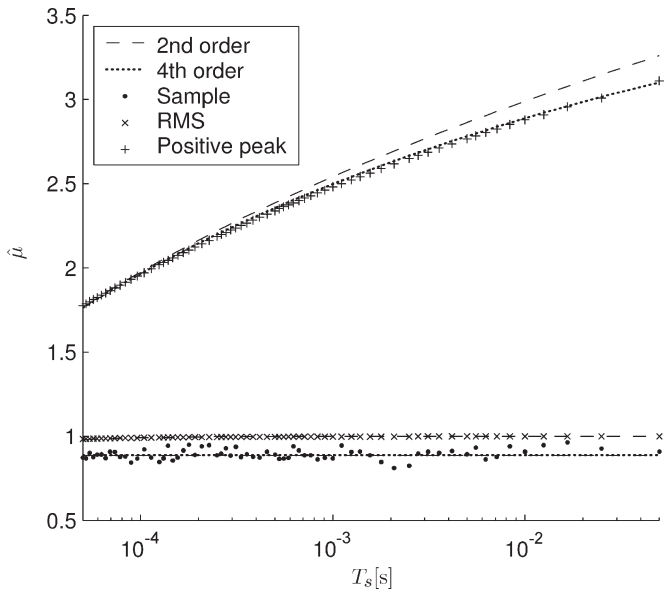

Fig. 5. Comparison between the expected values of the distribution of the measured UMTS signal for the different detector modes of a spectrum analyzer as a function of the length of the measurement period T_s. The levels have been normalized to the square root of the expected MS level. The chosen sweep time was 500 ms, the frequency span was 6 MHz, and the RBW was 100 kHz. For the rms detector, only the second-order approximation is given, and for the sample and positive-peak detector, the values obtained with both the second- and fourth-order approximation are shown. Simulation results are also indicated as a reference.

IV. Discussion

Now that the stochastic description of the WCDMA signal measured by a spectrum analyzer has been determined for the different detector modes, the behavior of the measured signals can be compared. As a summary, the dependence on the measurement period T_s of the mean and standard deviation of the measured signal level, respectively, are given in Figs. 5 and 6, respectively, for the different detector modes of the spectrum analyzer. The resolution filter was chosen as 100 kHz. The levels have been normalized to the square root of the MS level $\sqrt{T_c \sum_j g_j^2/(2\sqrt{\pi}\sigma_t)}$ and should be corrected with this level to obtain the correct power of the signal. The mean value of the sample detector is somewhat lower than the root of the MS level, and the standard deviation for the sample detector is the largest. The mean of the rms detector deviates slightly from 1 but approaches 1 for larger measurement periods T_s; the standard deviation of the rms detector decreases for larger measurement periods T_s and is smaller than the standard deviation of both the sample as the positive-peak detector. For the positive-peak detector, the mean increases with larger measurement periods, but the standard deviation decreases. It should be noted that, although the standard deviation of the peak detector is for small measurement periods of the same order as the standard deviation of the sample detector, the relative width of the PDF of the positive-peak detector will be much smaller due to its higher mean level. For longer simulation periods, the relative standard deviation becomes even smaller.

The predicted mean values agree very well with the simulated means for all detectors. The agreement between simulated and predicted standard deviations is rather good. For the rms detector, there is some divergence for short time periods, while for the positive-peak detector, the difference increases for larger measurement periods. The second-order approximation performs well for the sample and rms detector, while for the positive-peak detector, the inclusion of the fourth order is necessary to predict the mean value of the measured level.

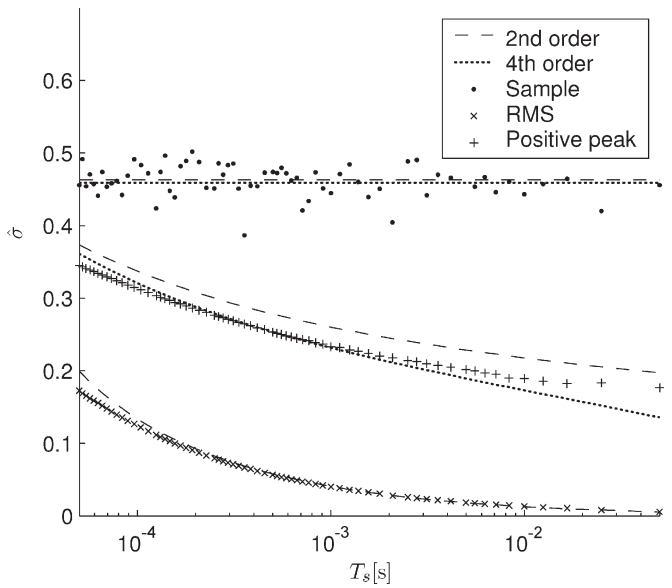

Fig. 6. Comparison between the standard deviation of the distribution of the measured UMTS signal for the different detector modes of a spectrum analyzer. The levels have been normalized to the square root of the expected MS level as a function of the length of the measurement period T_s. The chosen sweep time was 500 ms, the frequency span was 6 MHz, and the RBW was 100 kHz. For the rms detector, only the second-order approximation is given, and for the sample and positive-peak detector, the values obtained with both the second- and fourth-order approximation are shown. Simulation results are also indicated as a reference.

From Fig. 5, it appears that the mean rms level of the signal can be estimated from the mean level measured with the positive-peak detector through division of the measured positive-peak level with the value of $\hat{\mu}$, given in Fig. 5, for the positive-peak detector, at the appropriate measurement period T_s. This may be useful if there is no rms detector present in the spectrum analyzer. Another application is the estimation of the maximum rms level that has occurred for a WCDMA signal where the power levels are changing rapidly compared to the measuring period. In this case, the maximum power level could be estimated from the level measured with the positive-peak detector (using the time period of the power variation as "measuring period"), while the value returned by the rms detector would underestimate the maximum power level. It can be noted that the uncertainty on the measurement value is higher for the rms level estimated from the positive-peak detector compared to the level measured by the rms detector. If the measured signal level of the WCDMA signal is of the same order of magnitude of the noise floor of the spectrum analyzer, the curve of $\hat{\mu}$ for the positive-peak detector will tend more towards the second-order approximation. Hence, the derivation of the rms level, from the positive-peak value with the fourth-order curve, will imply an overestimation of the real rms level. It should also be noted that in the presence of noise, the measured signal will behave as a noise-free signal with a power level equal to the sum of the signal and the noise power. If the spectral density of the internal noise would be known, it is possible to estimate the power density present in the WCDMA signal by subtracting the noise power density, provided that the WCDMA signal is sufficiently stronger than the noise floor of the spectrum analyzer.

V. Conclusion

In this paper, the authors have determined, for the different detector modes, the behavior of the WCDMA signal measured by a spectrum analyzer. Analytical expressions for the PDFs or CDFs have been derived and have provided insight in both the characteristics of the signal and the operation of a spectrum analyzer. From these analytical expressions, the dependence on the measuring period of the mean measured level and of its standard deviation has been calculated. From the comparison, it appears that the rms detector is preferred to estimate the power of the WCDMA signal since it delivers the smallest standard deviation. It has also been shown that the rms level can be estimated from a positive-peak measurement if one takes into account the measuring period, although a higher uncertainty on the result is associated with this method. This is useful in the case where no rms detector is present in the spectrum analyzer or if one wants to measure the maximum power of a WCDMA signal with rapidly changing power levels. If the noise floor has the same order of magnitude as the measured signal level, the behavior of the measured sample and rms level will behave as if the power density of the WCDMA signal is increased with the noise power density. In the case where multiple equivalent WCDMA channels are active, or when the noise floor cannot be neglected compared to the WCDMA signal level, the behavior of the measured positive-peak level will resemble more the measurement of the white noise.

Appendix

As it was previously mentioned, (14) is only valid for arguments of the cosine function that are smaller than $\pi/2$. In this Appendix, the threshold is estimated above which (15) is no longer valid and where a continuous description of the stochastic behavior is no longer appropriate and, thus, only indicates the main course of the PDF.

To get an idea about the threshold between continuous and discrete behaviors, we will study the distribution of the real part of $s(t)$, i.e., before the envelope detector. Since the discrete behavior occurs due to the existence of a "side lobe" in the characteristic function, it is interesting to describe the characteristic function around the first next extremum of the cosine function with the largest argument, i.e., $u = \pm\pi\sqrt{2}/|g_{n_0}(n_0 T_\mathrm{c})|$. Here, the limit situation is considered where all pulse contribution functions are purely real or imaginary. The characteristic function can then be written as

$$\Psi_{S_\mathrm{r}}(u) = \prod_{k_0=-K_0}^{K_0} \cos\left(\frac{|p_{n_0+k_0}|}{\sqrt{2}}u\right) \prod_{k_1\notin[-K_0,K_0]} \cos\left(\frac{|p_{n_0+k_1}|}{\sqrt{2}}u\right) \tag{68}$$

$$\approx -\exp\left(-\frac{1}{2}\left(\pi \mp \frac{|p_{n_0}|}{\sqrt{2}}u\right)^2 - \sum_{k_0=1}^{K_0}\left(\pi \mp \frac{|p_{n_0+k_0}|}{\sqrt{2}}u\right)^2 - \sum_{k_1=K_0+1}^{\infty}\frac{|p_{n_0+k_0}|^2}{2}u^2\right) \tag{69}$$

where K_0 is the largest index of which the approximation around 0 (14) is not valid at $u = \pm\pi\sqrt{2}/|g_{n_0}(n_0 T_\mathrm{c})|$. This index can be determined as follows:

$$\frac{|g_{n_0+k_0}|}{\sqrt{2}}\frac{\sqrt{2}\pi}{|g_{n_0}|} \geq \frac{\pi}{2} \tag{70}$$

$$\exp\left(-\frac{k_0^2 T_\mathrm{c}^2}{2\sigma_\mathrm{t}^2}\right) \geq \frac{1}{2} \tag{71}$$

$$k_0 \leq \sqrt{2\ln 2}\frac{\sigma_\mathrm{t}}{T_\mathrm{c}} \tag{72}$$

where (11) has been applied. The largest index is thus given by $K_0 = \lfloor\sqrt{2\ln 2}\sigma_\mathrm{t}/T_\mathrm{c}\rfloor$, which can be approximated by the continuous variable $K_0 \approx \sqrt{2\ln 2}\sigma_\mathrm{t}/T_\mathrm{c} - 1/2$. The second extremum of the characteristic function will be given by

$$|\Psi_{S_\mathrm{r}}(u_{\max})| = \exp\left(-\frac{\pi^2}{2}\left((2K_0+1) - \frac{\left(\sum_{k=-K_0}^{K_0}|p_{n_0+k}|\right)^2}{\sum_{k=-\infty}^{+\infty}|p_{n_0+k}|^2}\right)\right). \tag{73}$$

The truncated sum can be approximated by applying the Poisson sum formula as

$$\sum_{k=-K_0}^{K_0}|g_{n_0+k}| \approx \sqrt{2\pi}\frac{\sigma_\mathrm{t}}{T_\mathrm{c}}\mathrm{erf}\left(\sqrt{\ln 2}\right) \tag{74}$$

which yields for the characteristic function

$$|\Psi_{S_\mathrm{r}}(u_{\max})| \approx \exp\left(-\pi^2 \frac{\sigma_\mathrm{t}}{T_\mathrm{c}}\left(\sqrt{2\ln 2}-\sqrt{\pi}\left(\mathrm{erf}(\sqrt{\ln 2})\right)^2\right)\right). \tag{75}$$

If it is assumed that the maximum level of the side lobe should be below 0.05, the threshold for the RBW can be determined as

$$\mathrm{RBW} > \frac{\pi\left(\sqrt{2}\ln 2 - \sqrt{\pi \ln 2}\left(\mathrm{erf}\left(\sqrt{\ln 2}\right)^2\right)\right)}{|\ln 0.05|}\frac{1}{T_\mathrm{c}} \tag{76}$$

$$> \frac{0.395}{|\ln 0.05|}\frac{1}{T_\mathrm{c}} \approx 500\ \mathrm{kHz}. \tag{77}$$

REFERENCES

[1] International Commission on Non-Ionizing Radiation Protection (ICNIRP), "Guidelines for limiting exposure to time-varying electric, magnetic, and electromagnetic fields (up to 300 GHz)," *Health Phys.*, vol. 74, no. 4, pp. 494–594, Apr. 1998.

[2] *IEEE Standard for Safety Levels With Respect to Human Exposure to Radio Frequency Electromagnetic Fields, 3 kHz–300 GHz*, IEEE Std. C95.1-1991, 1999.

[3] European Council, "Council recommendation of 12 July 1999 on the limitation of exposure of the general public to electromagnetic fields (0 Hz–300 GHz)," *Off. J. Eur. Communities*, vol. 42, no. L199, pp. 59-70, 1999.

[4] C. Olivier and L. Martens, "A practical method for compliance testing of base stations for mobile communications with exposure limits," in *Proc. IEEE Antennas and Propagation Society/URSI Symp.*, Boston, MA, Jul. 8–13, 2001, vol. 2, pp. 64–67.

[5] G. Neubauer, H. Haider, and K. Lamedschwandner, "Measurement methods and legal requirements for exposure assessment next to GSM base stations," in *Proc. 15th Int. Zurich Symp. Electromagnetic Compatibility*, Zurich, Switzerland, Feb. 18–20, 2003, pp. 143–148.

[6] *Basic Standard for the Calculation and Measurement of Electromagnetic Field Strength and SAR Related to Human Exposure From Radio Base Stations and Fixed Terminal Stations for Wireless Telecommunication Systems (110 MHz–40 GHz),* CENELEC Std. EN 50 383:2002, 2002.

[7] *Product Standard to Demonstrate the Compliance of Radio Base Stations and Fixed Terminal Stations for Wireless Telecommunication Systems With the Basic Restrictions or the Reference Levels Related to Human Exposure to Radio Frequency Electromagnetic Fields (110 MHz–40 GHz)—Occupational,* CENELEC Std. EN 50 384:2002, 2002.

[8] *Product Standard to Demonstrate the Compliance of Radio Base Stations and Fixed Terminal Stations for Wireless Telecommunication Systems With the Basic Restrictions or the Reference Levels Related to Human Exposure to Radio Frequency Electromagnetic Fields (110 MHz–40 GHz)—General Public,* CENELEC Std. EN 50 385:2002, 2002.

[9] *Basic Standard for the Calculation and Measurement of Electromagnetic Fields Related to Human Exposure From Radio Base Stations and Fixed Terminal Stations for Wireless Telecommunication Systems (110 MHz–40 GHz), When Put Into Service,* CENELEC Std. prEN 50 400:2004, 2004.

[10] *Product Standard to Demonstrate the Compliance of Radio Base Stations and Fixed Terminal Stations for Wireless Telecommunication Systems With the Basic Restrictions or the Reference Levels Related to General Public Human Exposure to Radio Frequency Electromagnetic Fields (110 MHz–40 GHz), When Put Into Service,* CENELEC Std. prEN 50 401:2004, 2003.

[11] C. Olivier and L. Martens, "Optimal settings for narrow band signal measurements used for exposure assessment around GSM base station antennas," *IEEE Trans. Instrum. Meas.*, vol. 54, no. 1, pp. 311–317, Feb. 2005.

[12] C. Rauscher, *Fundamentals of Spectrum Analysis*. München, Germany: Rohde and Schwarz, 2001.

[13] H. Holma and A. Toskala, Eds., *WCDMA for UMTS*. West Sussex, U.K.: Wiley, 2000.

[14] *Radio Access Networks; User Equipment (UE) Radio Transmission and Reception (FDD) (release 1999),* ETSI/3GPP Std. TS 25.101, 2005.

[15] *Radio Access Networks; BS Radio Transmission and Reception (FDD) (release 1999),* ETSI/3GPP Std. TS 25.104, 2005.

[16] *Group Radio Access Network; Physical Layer—General Description (Release 1999),* ETSI/3GPP Std. TS 25.201, 2002.

[17] *Radio Access Network; Spreading and Modulation (FDD) (Release 1999),* ETSI/3GPP Std. TS 25.213, 2003.

[18] *Digital Cellular Telecommunications System (Phase 2+); Modulation,* ETSI/3GPP Std. TS 05.04, 2001.

[19] M. Abramowitz and I. A. Stegun, *Handbook of Mathematical Functions*. Boulder, CO: National Bureau of Standards, 1972.

[20] H. Ochiai and H. Imai, "On the distribution of the peak-to-average power ratio in OFDM signals," *IEEE Trans. Commun.*, vol. 49, no. 2, pp. 282-289, Feb. 2001.

[21] S. O. Rice, "The distribution of the maxima of a random curve," *Amer. J. Math.*, vol. 61, no. 2, pp. 409–416, Apr. 1939.

Christof Olivier was born in Izegem, Belgium, on September 24, 1976. He received the M.Sc. degree in electrical engineering from Ghent University, Ghent, Belgium, in 1999 and is currently working toward the Ph.D. degree at the Department of Information Technology (INTEC), Ghent University.

From 1999 to 2005, he worked on electromagnetic-field measurements around base stations for mobile communications related to the health effects of the exposure to electromagnetic radiation. His research interests are in electromagnetic-field measurements, antennas, and propagation. Since February 2005, he has been working at tComLabs, Ghent, on broadband wireless access systems.

Luc Martens (M'92) was born in Ghent, Belgium, on May 14, 1963. He received the M.Sc. degree in electrical engineering from Ghent University in 1986 and the Ph.D. degree from the same university in 1990, where his scientific work focused on the physical aspects of hyperthermic cancer therapy and dealt with electromagnetic and thermal modeling and development of measurement systems for that application.

From September 1986 to December 1990, he was a Research Assistant at the Department of Information Technology (INTEC), Ghent University. Since January 1991, he has been a member of the permanent staff of the Interuniversity MicroElectronics Centre (IMEC), Ghent, and is responsible for the research on experimental characterization of the physical layer of telecommunication systems at INTEC. His group also studies topics related to the health effects of wireless communication devices. Since April 1993, he has been a Professor of electrical applications of electromagnetism at Ghent University.